International Journal of Hydrogen Energy 80 (2024) 733–742

Contents lists available at ScienceDirect

International Journal of Hydrogen Energy

journal homepage: www.elsevier.com/locate/he

A parametric study on in-situ hydrogen production from hydrocarbon reservoirs – Effect of reservoir and well properties

Princewill Ikpeka [a,*], Emmanuel Alozieuwa [b], Ugochukwu I. Duru [c], Johnson Ugwu [d]

[a] Global Challenges and Transdisciplinary Change, Brunel University, Uxbridge, United Kingdom
[b] Natwest Building Society
[c] Department of Petroleum Engineering, Federal University of Technology, Owerri, Nigeria
[d] School of Computing Engineering and Digital Technologies, Teesside University, Middlesbrough, United Kingdom

ARTICLE INFO

Handling Editor: Dr V Palma

ABSTRACT

Energy transition is a key driver to combat climate change and achieve zero carbon future. Sustainable and cost-effective hydrogen production will provide valuable addition to the renewable energy mix and help minimize greenhouse gas emissions. This study investigates the performance of in-situ hydrogen production (IHP) process, using a full-field compositional model as a precursor to experimental validation The reservoir model was simulated as one geological unit with a single point uniform porosity value of 0.13 and a five-point connection type between cell to minimize computational cost. Twenty-one hydrogen forming reactions were modelled based on the reservoir fluid composition selected for this study. The thermodynamic and kinetic parameters for the reactions were obtained from published experiments due to the absence of experimental data specific to the reservoir. A total of fifty-four simulation runs were conducted using CMG STARS software for 5478 days and cumulative hydrogen produced for each run was recorded. Results generated were then used to build a proxy model using Box-Behnken design of experiment method and Support Vector Machine with RBF kernel. To ascertain accuracy of the proxy models, analysis of variance (ANOVA) was conducted on the variables. The average absolute percentage error between the proxy model and numerical simulation was calculated to be 10.82%. Optimization of the proxy model was performed using genetic algorithm to maximize cumulative hydrogen produced. Based on this optimized model, the influence of porosity, permeability, well location, injection rate, and injection pressure were studied. Key results from this study reveals that lower permeability and porosity reservoirs supports more hydrogen yield, injection pressure had a negligible effect on hydrogen yield, and increase in oxygen injection rate corelated strongly with hydrogen production until a threshold value beyond which hydrogen yield decreased. The framework developed in the study could be used as tool to assess candidate reservoirs for in-situ hydrogen production.

1. Introduction

The world's energy demand is projected to grow due to population growth, urbanization, and industrialization. Fossil fuels have been the primary source of energy for the past 150 years, and their use has contributed to environmental issues such as air pollution, greenhouse gas emissions, and climate change. To preserve the earth's environment and biodiversity, it is critical then to find more sustainable energy sources that matches projected energy demand growth [1]. Hydrogen is an essential energy carrier that can potentially replace fossil fuels, mitigate greenhouse gas emissions, and support the transition to a low-carbon economy. However, current hydrogen production methods based on steam methane reforming (SMR) are energy intensive, consume lots of clean water and produce substantial CO_2 as by-products [2,3]. Supported by funding from both industry/government, several studies have been made exploring alternative ways of producing cheaper Hydrogen (H_2) while sequestering the accompanying carbon dioxide (CO_2) and Carbon monoxide (CO). Gillick and Babaei [4] proposed a system that gasifies natural gas within a downhole completion tool installed at the wellbore, that converts methane wells into hydrogen production wells. Other researchers focus on extending conventional in-situ combustion (for heavy oils/Bitumen) process to achieve

* Corresponding author.
E-mail address: princewill.ikpeka@brunel.ac.uk (P. Ikpeka).

https://doi.org/10.1016/j.ijhydene.2024.07.180
Received 25 December 2023; Received in revised form 6 July 2024; Accepted 12 July 2024
Available online 17 July 2024

hydrogen production via gasification [5–9]. A few other studies have been published investigating the use of microwave and electromagnetic heating to generate hydrogen in petroleum reservoir in-situ [10,11]. In-situ hydrogen production (IHP) presents an interesting solution to this problem. During in-situ hydrogen production process, oxygen (or oxygen-enriched air) is introduced to the hydrocarbon reservoir to initiate both exothermic and endothermic reactions. The heat released from the exothermic reactions supplements the energy needed by the endothermic reactions to produce hydrogen. A graphical illustration of the IHP process is captured by Fig. 1. Hydrogen is produced via any number of reactions at the elevated reservoir pressure and temperature condition: aqua thermolysis, thermolysis, coke gasification, water-gas shift reaction and methanation [12]. At the subsurface, hydrogen and other valuable gases are then extracted using permeable membranes, while leaving behind CO_2 and other undesired gases.

Field-scale tests conducted in the past for in-situ combustion have also demonstrated the feasibility of producing hydrogen in-situ as well; 14% hydrogen content reported by [42] in 1977, while Marguerite Lake and Wolf Lake ISC projects operated by bp reported hydrogen contents of 33 mol.% and 25 mol.% respectively [12,13]. In-situ hydrogen has the potential to harness extensive hydrocarbon reserves that have been deemed unrecoverable, as it provides a cost effective and sustainable method for utilizing these depleted reservoirs while generating energy in the form of hydrogen. One significant advantage of this approach is that the CO_2 produced can be separated at the source, eliminating the need for dedicated facilities for CO_2 transportation and storage [14]. Another strong appeal for this method is that it offers a cost-effective solution for hydrogen production when compared to the existing hydrogen production methods because it leverages on existing assets deployed in the field and limits the need for additional infrastructures [15,16]. In addition, the process has the potential to reduce emissions, which is advantageous for both the environment and public health. This is primarily achieved through controlled conditions during the process, which allows for the simultaneous sequestration of impurities while producing hydrogen [16]. However, the drawback of this advantage is that there is a potential for significantly reduced conversion efficiency, coupled with limited control over the chemical reactions occurring beneath the surface.

Similar to conventional in-situ combustion process, IHP process is dependent on several factors, some of which include reservoir rock mineralogy [17], combustion temperature & pressure [8,18], hydrocarbon composition [16,19], air/oxygen injection ratio [20] and injection strategy [9,17]. Temperature and pressure have an important effect on chemical reactions and subsequent molecular motions. During hydrocarbon combustion higher temperature improves speed of molecular motion, boosts effective molecule collision, and subsequently leads to increase in reaction rates. In a lab scale simulation study by Song et al. [8], hydrogen yield increased from 2% to 30% when the injection temperature increased from 100 to 400 °C. The carbon activity during steam methane reforming is closely related to the position of the reaction equilibrium, i.e., higher temperature shifts equilibrium more towards hydrogen and carbon oxide production. This implies that higher reaction temperatures lead to higher hydrocarbon conversion and hydrogen output regardless of the presence of catalyst [21]. However, as the pressure increases with reaction temperature, the reservoir pore structure may be altered. Changes in the rock mineralogy may follow as more carbon deposits on the pore spaces. In addition, at higher temperature, catalyst present in the clay deactivates rapidly because carbon deposits (formed as an after-effect of increased forward reaction rate) block active sites on the catalyst surface and this decreases the effectiveness of the catalyst.

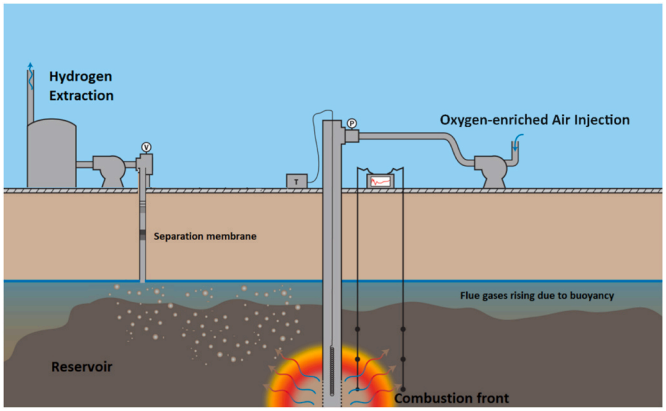

Fig. 1. Simplified illustration of the IHP process. Image adapted from [36].

Reservoir geology encompasses a range of subsectors; petrophysical and geophysical properties, rock mineralogy, reservoir stratigraphy and sediment deposition patterns and heterogeneities such as fractures, channels, or layered systems. Each of these properties influence either positively or negatively the hydrogen yield obtained during in-situ hydrogen process. Sandstone reservoirs are the most common targets for in-situ combustion (ISC) projects [22]. Virtually all sandstone reservoirs contain fractions of clay minerals. Although fine-grained clay minerals are detrimental to reservoir quality especially because it decreases porosity and permeability by blocking pore space, they have been found to be beneficial in some cases. Some clay minerals alter the in-situ combustion rate by lowering the activation energy and catalysing fuel oxidation (coke deposition) as result of high surface area of the clay particles [23,24]. In addition, variations in reservoir thickness can influence the in-situ process. For example, thinner reservoirs lead to greater heat loss, resulting in the need for higher air-oil ratios, and lower combustion front temperatures [25].

The composition of hydrocarbon within the reservoir pore space also affects the hydrogen yield of the in-situ hydrogen production process [26,27]. The nature of the combustion front, the amount of heat released, and the overall temperature increase during combustion are all dependent on the hydrocarbon composition in the reservoir [18,28–30]. Hydrocarbon properties can be classified into several categories based on API gravity (density), viscosity, or chemical composition. The hydrocarbon viscosity is dependent on the composition, reservoir temperature and pressure. An important effect of viscosity on an IHP process is coke (solids) deposition. A series of combustion tube experiments conducted on five different crude oils, with API gravity ranging from 10° to 36°, revealed that coke production increased as viscosity increased and API gravity decreased [5,31,32]. Activation energy required for thermal reactions is also dependent on the API gravity of the hydrocarbon. In another study by Kok and Keskin [33] using three hydrocarbon samples between 13° and 27° API, it was shown that heavier hydrocarbons had lower activation energy for coke deposition.

In an earlier study [19], we developed a combustion model to characterize the effect of steam composition, oxygen composition, pressure, and temperature on hydrogen yield based on four hydrogen forming reactions – steam reforming, partial oxidation, autothermal reforming and pyrolysis. However, there is a need to understand the influence of reservoir and well parameters on the amount of hydrogen produced [17,26]. In this study, we evaluated the importance of 6 well/reservoir parameters using thermal model of a sandstone reservoir developed on CMG STARS. The 6 factors identified as variables to be studied are porosity, permeability, well location (I-location, and J-location), injection rate and injection pressure. Due to the absence of well-designed laboratory experiments, there are still no comprehensive reaction models to describe the influence of these factors on hydrogen yield. This study attempts to address this critical gap by employing the use of numerical simulation as a precursor to conducting laboratory experiments. The novelty of this study lies in its integration of numerical simulations and proxy modelling to predict the impact of reservoir and well properties on hydrogen yield, which could serve as a precursor to conducting actual experiments. In addition, the study aims to establish

directionally, the influence of these reservoir and well properties on optimum hydrogen yield during the IHP process.

2. Methodology

The initial step entails reproducing a functional reservoir model for the numerical simulation. To do this, a cartesian grid type reservoir model with dimensions consistent with the model used by Kenyon [34] was adapted for the in-situ hydrogen production study. The reservoir grid structure is made up of 9 cells in the i-direction, 9 Cells in the j-direction and 4 cells in the k-direction as shown in Fig. 2. To simplify the model and minimize computational cost, the entire reservoir grid is simulated as one geological unit with a single point uniform porosity value of 0.13 and a five-point connection type between each cell.

This means at any point in the hydrostatic pressure regime is in a state of equilibrium. A summary of the reservoir data is provided in Table 1 and the PVT data matched for both constant volume depletion and constant composition expansion experiments.

To initiate combustion during the IHP process, oxygen is injected into the reservoir model via the injection well located at (1i, 9j), completed at layer (3-4k) in the k-direction. Hydrogen and other flue gases are then produced at the production well located at (7i, 3j), completed at layers (3-4k). PVT data used in this study were adapted to match fluid composition used by Kenyon [34]. Based on the reservoir fluid composition and the change in Gibbs Free Energy during the IHP process, 21 hydrogen forming reactions were modelled according to Ikpeka and Ugwu [19]. The hydrogen forming reactions include:

$$1.232O_2 + Coke \rightarrow 0.564\,H_2O + 0.8995CO_2 + 0.1CO \quad (1)$$

$$CH_4 + 2O_2 \rightarrow 2H_2O + CO_2 \quad (2)$$

$$Gas + 2O_2 \rightarrow 2\,H_2O + CO_2 + 0.9695CO \quad (3)$$

$$H_2O + Coke \rightarrow CO + 1.558\,H_2 \quad (4)$$

$$CO + 1.558\,H_2 \rightarrow H_2O + Coke \quad (5)$$

$$H_2O + CO \rightarrow CO_2 + H_2 \quad (6)$$

$$CO_2 + H_2 \rightarrow H_2O + CO \quad (7)$$

$$2H_2 + Coke \rightarrow 1.068\,CH_4 \quad (8)$$

$$1.068\,CH_4 \rightarrow 2H_2 + Coke \quad (9)$$

$$CO + 0.5O_2 \rightarrow CO_2 \quad (10)$$

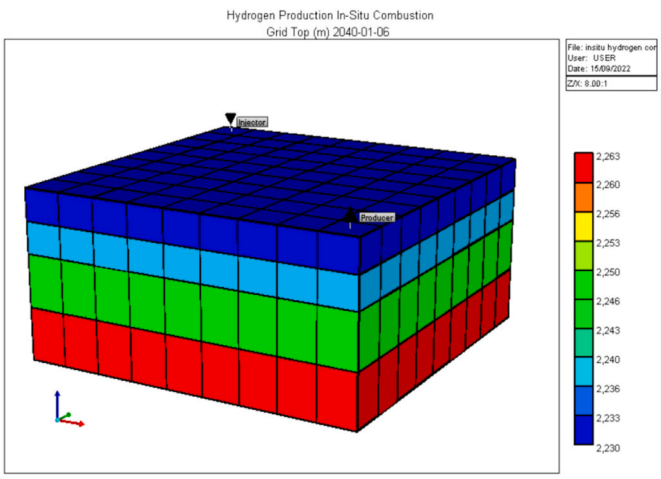

Fig. 2. Reservoir grid structure for the in-situ hydrogen production study.

$$H_2 + 0.5O_2 \rightarrow H_2O \quad (11)$$

$$O_2 + C_2H_6 \rightarrow 3H_2 + 2CO \quad (12)$$

$$1.5\,O_2 + C_3H_8 \rightarrow 4H_2 + 3CO \quad (13)$$

$$2O_2 + C_4H_{10} \rightarrow 5H_2 + 4CO \quad (14)$$

$$2.5\,O_2 + C_5H_{12} \rightarrow 6H_2 + 5CO \quad (15)$$

$$3\,O_2 + C_6H_{14} \rightarrow 7H_2 + 6CO \quad (16)$$

$$3.5\,O_2 + C_7H_{16} \rightarrow 8H_2 + 7CO \quad (17)$$

$$4\,O_2 + C_8H_{18} \rightarrow 9H_2 + 8CO \quad (18)$$

$$5\,O_2 + C_{10}H_{22} \rightarrow 11H_2 + 10CO \quad (19)$$

$$H_2O + CH_4 \rightarrow 3H_2 + CO \quad (20)$$

$$2H_2O + C_2H_6 \rightarrow 5H_2 + 2CO \quad (21)$$

These reactions were simulated using a thermal reservoir simulator [43] to calculate the overall amount of hydrogen produced through the IHP process. The simulator uses a finite volume method to solve the energy balance, considering conductive and convective heat transfer, as well as the mass balance of various components, accounting for diffusive and advective mass transfer. These calculations are performed for each reaction listed in equations (1)–(21). The rate at which each reaction occurs during the IHP depends on the temperature, which is determined using the Arrhenius relationship described in equation (22).

$$K_{reaction} = Ae^{\frac{-E}{RT}} \quad (22)$$

Where: A is the frequency factor, E is the activation energy, and R is the universal gas constant.

Ideally, the parameters needed to calculate the Arrhenius rate of reaction should be determined through laboratory experiments. However, since there are no experimental data available for this specific reservoir, data from previously published literature were utilized to estimate the reaction rates. The specific sources of data used to calculate the rates of each reaction are provided in Table 2.

To understand the influence of reservoir and well parameters on the amount of hydrogen produced, the following variables: porosity, permeability, well location (I-location, and J-location), injection rate and injection pressure, would be optimized. The minimum and maximum values for each level were chosen to reflect realistic values of the reservoir, to avoid impractical values of high/low and eliminate extreme and impossible combinations with other factors in the design of experiment (DoE). The input parameters used for the analysis are outlined in Table 3.

The response (output) parameter required from the simulator is cumulative hydrogen produced (CHP). CHP was selected to align with the objective of the IHP process which is to optimize total hydrogen produced as shown in equation (23).

$$CHP = f(X_1, X_2, X_3, X_4, X_5, X_6) \quad (23)$$

Where: CHP – cumulative hydrogen produced, $X_{1\text{-}6}$ – input parameter being investigated.

The 6 factors identified could be further categorized into 3 main group: Well control parameters (injection rate, injector pressure), Well-placement parameters (producer location {i,j}), and reservoir parameters (porosity and permeability). CMG STARS® was used for full field reservoir simulation, and Design Expert® was used for design of experiment. The results generated from the simulation runs were used to build the proxy model. An analysis of variance (ANOVA) was conducted on the model to verify its accuracy relative to the numerical simulations.

Table 1
Reservoir grid data.

Parameter (unit) Value
$N_X = N_Y = 9$, $N_Z = 4$
$D_X = D_Y = 293.3$ ft
Datum (subsurface), ft 7500 ft
Porosity (at initial reservoir pressure) 0.13
Gas/water contact, ft 7500 ft
Water saturation at contact 1.00
Capillary pressure at contact 0 psia
Initial pressure at contact 3550 psia
Water density at contact 63.0 lbm/ft^3
Water compressibility 3.0 × 10^{-6} psi^{-1}
PV compressibility 4.0 × 10^{-6} psi^{-1}

Layer	Horizontal Permeability	Vertical Permeability	Thickness (ft)	Depth to Center (ft)
1	130	13	30	7330
2	40	4	30	7360
3	20	2	50	7400
4	150	15	50	7450

Table 2
Parameters for Arrhenius reaction extracted from published literature.

Reaction	Reaction Frequency Factor	Enthalpy (-ve for endothermic reactions) [J]	Activation Energy (EACT) [J/mol]	Source
1	3.881 x 10^0	3.946 x 10^5	8.205 x 10^2	[38]
2	3.020 x 10^{10}	8.910 x 10^5	5.945 x 10^4	[39]
3	1.311 x 10^8	4.436 x 10^5	2.662 x 10^5	
4	2.117 x 10^7	−1.314 x 10^5	9.20 x 10^4	[40]
5	5.291 x 10^2	1.314 x 10^5	3.46 x 10^4	[12]
6	5.573 x 10^7	4.10 x 10^4	1.49 x 10^5	
7	4.29 x 10^9	−4.1 x 10^4	1.90 x 10^5	
8	3.162 x 10^4	7.489 x 10^4	4.14 x 10^4	[40]
9	7.113 x 10^9	−7489 x 10^4	1.163 x 10^5	
10	1.123 x 10^7	2.830 x 10^5	1.255 x 10^5	[41]
11	8.986 x 10^7	2.860 x 10^5	1.255 x 10^5	
12	2.990 x 10^{10}	1.363 x 10^5	6.004 x 10^4	Modified from reaction 2
13	2.960 x 10^{10}	2.277 x 10^5	6.064 x 10^4	
14	2.929 x 10^{10}	3.159 x 10^5	6.123 x 10^4	
15	2.899 x 10^{10}	4.061 x 10^5	6.183 x 10^4	
16	2.869 x 10^{10}	4.643 x 10^5	6.242 x 10^4	
17	2.839 x 10^{10}	5.445 x 10^5	6.302 x 10^4	
18	2.809 x 10^{10}	6.339 x 10^5	6.361 x 10^4	
19	2.778 x 10^{10}	8.050 x 10^5	6.421 x 10^4	
20	2.117 x 10^7	−2.061 x 10^5	9.20 x 10^4	
21	2.117 x 10^7	−3.473 x 10^5	9.20 x 10^4	

Table 3
Input parameter range for the Box-Behnken design.

Parameter	Unit	Symbol	Low Case	Mid Case	High Case
Porosity	%	X_1	10	20	30
Horizontal Permeability	md	X_2	20	100	200
Producer location (i)	–	X_3	1	5	9
Producer location (j)	–	X_4	2	5	9
Injection rate	m^3/day	X_5	500	750	1000
Injection pressure (BHP)	kPa	X_6	24131.66	32750.1	41368.51

Finally genetic algorithm in MATLAB was used to optimize the developed proxy model, aiming to determine the optimum values of reservoir/well parameters that will maximize hydrogen yield for the in-situ hydrogen production study. This process is summarized by the flowchart given in Fig. 3.

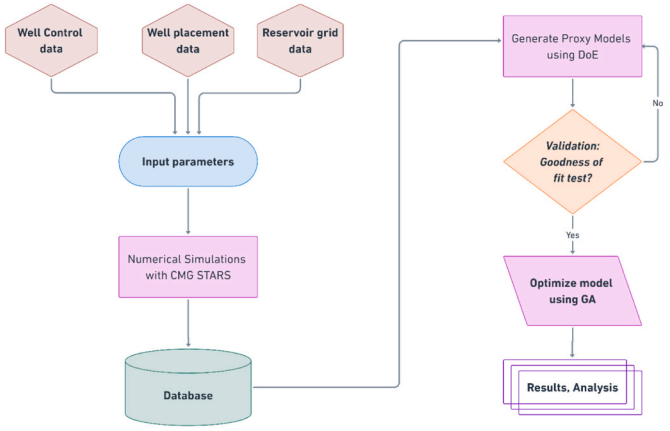

Fig. 3. Methodology employed to optimize proxy model.

3. Analysis

Due to the large number simulation runs that will be required to optimize the model, it is impractical to run direct optimization on CMG STARS® due to computational cost. Using the data ranges for each scenario shown in Table 3, parameter realizations for running reservoir simulations were generated using Box Behnken design of experiment. In the Box-Behnken design the levels of each factor are given at the mid-points of the edges (red dots) and in the centre (blue dot) as shown in Fig. 4. For each factor are 3 levels required: low case, mid case, and high case.

For the six (6) variables, a total of 54 simulation runs were conducted and the cumulative hydrogen produced during each run were measured. Each simulation ran for 5478 days, and the cumulative hydrogen produced for each run is presented in Table A1 in the appendix section. Analysing the result from each of the 54 scenarios shows that the maximum and minimum CHP after 5478 days of production are 3.29E+05 m^3 and 1.45E+03 m^3 respectively. The time series plot of each CHPs is given in Fig. 5.

The CHP for each scenario in combination with the respective input parameters were analysed using design of experiment to generate a proxy model. The variables of the proxy model can be categorized into 3 components: linear, interaction and quadratic components. Results from the analysis of variance for the proxy model is given in Table 4. Results from the analysis of variance (ANOVA) reveal that not all variables were significant to the model i.e., p-value greater than 0.05.

To minimize the model size, terms with p-value lower than 0.05 (i.e., statistically significant variables) were isolated from the rest of the parameter. However, injection pressure (X_6) with a p-value of 0.956 which is greater than 0.05, was allowed in the proxy model to support hierarchy. The proxy model generated is presented by equation (24):

$$CHP = aX_1 + bX_2 + cX_3 + dX_4 + eX_5 + fX_6 + g(X_1 . X_4) + h(X_1 . X_5) + i(X_2 . X_4) + j(X_2 . X_5) + k(X_3 . X_4) + l(X_4 . X_5) + m(X_1)^2 + n(X_2)^2 + q(X_5)^2 + P \quad (24)$$

Where: $X_{1\text{-}6}$ – input parameter being investigated, P = −290842.07, and the lower-case alphabets are coefficients having the following values.

a	15966.63	*e*	915.52	*i*	−41.04	*m*	−282.73
b	−651.43	***f***	−0.03	***j***	0.42	***n***	1.35
c	−5734.62	***g***	−342.01	***k***	−705.41	q	−0.27
d	15238.5	***h***	−10.07	***l***	−15.83		

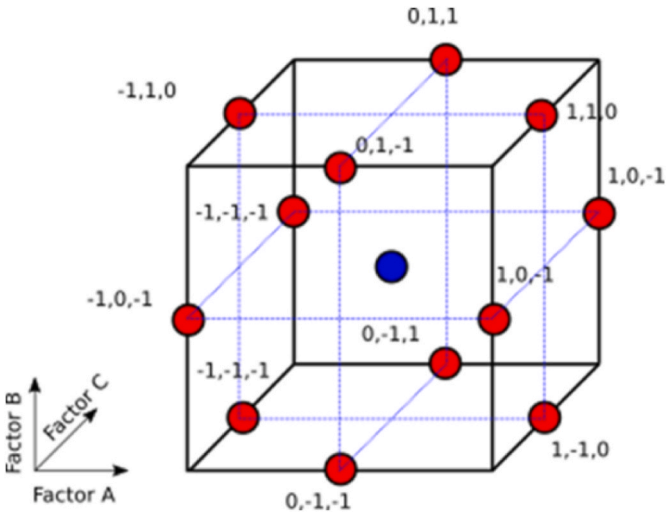

Fig. 4. Box-behnken design of experiment [37].

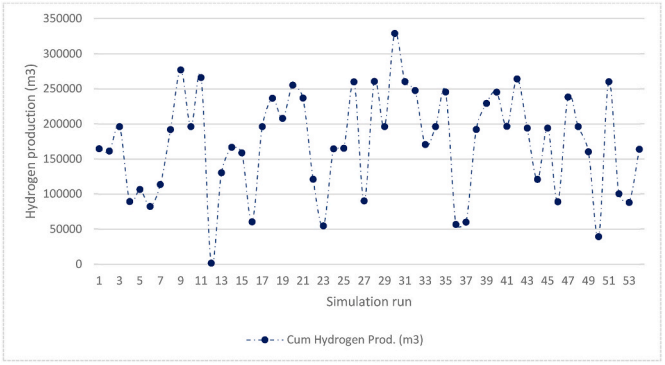

Fig. 5. Time series control chart for Cumulative hydrogen produced.

Table 4
Analysis of variance for the DOE Proxy model.

	Coefficient	Standard error	T-value	p-value	Significant
Constant	−290842	84325.17	−3.449	0.001	*
X_1	15966.63	3160.402	5.052	0	*
X_2	−651.43	262.762	−2.479	0.018	*
X_3	−5734.62	2737.697	−2.095	0.043	*
X_4	15238.5	7436.447	2.049	0.047	*
X_5	915.52	160.613	5.7	0	*
X_6	−0.03	0.466	−0.055	0.956	
X_1. X_4	−342.01	139.921	−2.444	0.019	*
X_1. X_5	−10.07	2.78	−3.622	0.001	*
X_2. X_4	−41.04	21.824	−1.88	0.068	
X_2. X_5	0.42	0.218	1.916	0.063	
X_3. X_4	−705.41	493.032	−1.431	0.161	*
X_4. X_5	−15.83	7.889	−2.007	0.052	*
$(X_1)^2$	−282.73	55.475	−5.096	0	*
$(X_2)^2$	1.35	0.743	1.816	0.077	*
$(X_5)^2$	−0.27	0.095	−2.882	0.006	*

3.1. SVM with radial basis function (RBF) kernel

A second method was used to generate proxy model using SVM with an RBF kernel. The SVM-RBF proxy model uses hidden layer of neurons, each associated with a radial basis function, to transform the input features into a higher -dimensional space where the parameters can be easily approximated by a quadratic model [35]. In this case, input features; porosity (%), permeability (md), P_i, P_J, Inj_Rate (m^3/day), and Inj_Press (kPa) were used to estimate the Cumulative Hydrogen produced (m^3). To generate the proxy model, we denote the input features as X. Each input feature of X is then used to generate a radial basis function as shown in equation in equation (25)

$$X = [x_1, x_2, x_3, x_4, x_5, x_6], \varnothing_i(X) = exp\left(- \frac{\|X - C_i\|^2}{2\sigma_i^2} \right) \quad (25)$$

Where.

- C_i is the center of the iii-th RBF neuron.
- σ_i is the spread (width) of the iii-th RBF neuron.
- $X - C_i$ is the Euclidean distance between the input vector X and the centre C_i.

The detailed algorithm is shown in Table 5.

3.2. Validation of proxy model

It is important to ensure that the proxy model is representative of the numerical model with minimal deviations. To confirm this, we validated the proxy model by comparing actual CHP (from simulator) to predicted CHP (from proxy model) using the coefficient of determination, R^2. Additionally, we calculated Root Mean Square Error (RMSE) and Average Absolute Percentage Error (AAPE) using equations (26) and (27).

$$RMSE = \sqrt{\sum_{i=1}^{n} \frac{(Simulated\ CHP_i - Proxy\ model\ CHP_i)^2}{n}} \quad (26)$$

$$AAPE = \frac{1}{n} \sum_{i=1}^{n} \left| \frac{Simulated\ CHP_i - Proxy\ model\ CHP_i}{Simulated\ CGP_i} \right| \quad (27)$$

The DOE proxy model had an RMSE of 1.64E+05 m^3 and an AAPE of 10.82%, whereas the SVM-RBF model had a higher RMSE of 3.11E+05 m^3 and a significantly higher AAPE of 21.4%. The DOE proxy model is clearly more suitable for this application, as it demonstrates much lower error values in both RMSE and AAPE compared to the SVM-RBF model. A potential reason for this difference may be due to the sample size. The analysis was conducted using a dataset of 47 samples, which may not have been sufficient for the SVM-RBF proxy model to characterize the RBF neurons. A plot of actual vs. predicted cumulative gas produced, and actual and predicted versus simulation runs are shown in Figs. 6 and 7 respectively.

3.3. Optimization

The more accurate proxy model (DOE proxy model) relating the

Table 5
Algortihm for generating SVM-RBF proxy model.

$\mathbb{N}$	Number of dataset available, $\mathbb{N} = \{1, \ldots, n\}$
X	Input matrix, $X = [x_1, x_2, x_3, x_4, x_5, x_6]$
C_i	Centre of the ith RBF neuron.
σ_i	Spread (width) of the ith RBF neuron.
$\hat{y}$	Vector of predicted values (Cum Hydrogen Produced (m3))
Φ_{ij}	RBF Matrix
1: for each input X_i and each neuron $\varnothing_j$	
2	$\boldsymbol{\Phi}_{ij} = \varnothing_j(\boldsymbol{X}_i) = exp\left(- \frac{\|\boldsymbol{X}_i - C_j\|^2}{2\sigma_j^2} \right)$
3	Solve for weights and biases
4	$\hat{\boldsymbol{y}} = \boldsymbol{\Phi w} + b$
5	$[\boldsymbol{w}, b] = \min_{w,b} \|y - (\boldsymbol{\Phi w} + b)\|^2$
6	Prediction
7	$\hat{\boldsymbol{y}}(X) = \sum_{i=1}^{\mathbb{N}} w_i\ exp\left(- \frac{\|\boldsymbol{X}_i - C_j\|^2}{2\sigma_j^2} \right) + b$
8	End

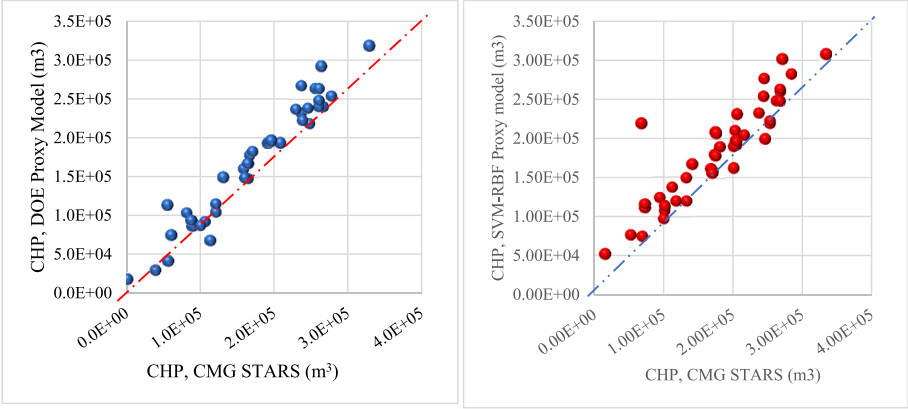

Fig. 6. Cross plot of the proxy model vs simulated CGP.

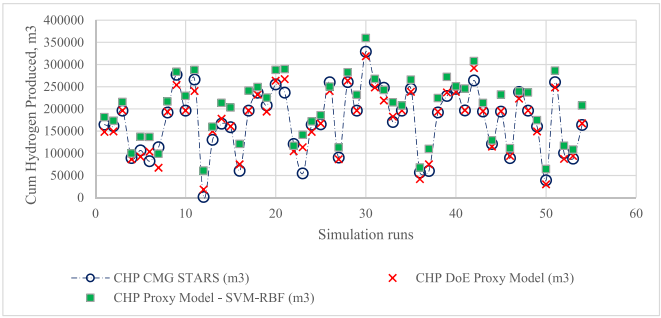

Fig. 7. Simulated and proxy model CHP plot against simulation runs.

response variable to the input parameters was modelled as non-linear objective functions subject to lower and upper bound constraints. Several optimization techniques could be applied to maximize the objective function, however genetic algorithm was chosen because of its stochastic non-derivative approach to obtaining the global maximum. Genetic algorithms make use of heuristic search techniques that mimic the process of natural evolution to produce successive high-quality solutions based on an initial population. We implemented genetic algorithm using the MATLAB global optimization toolbox and the objective was set to maximize the response variable for each proxy models. The outline of the genetic algorithm employed in this study is shown in Fig. 8. The quality of the solution obtained from the genetic algorithm optimization is dependent on; size of population, number of generations, crossover rate, and mutation rate between parents and offspring's solution space. To ensure repeatability of the solution, the value of these parameters used for the genetic algorithm and the results of the optimization are given in Table 6.

4. Results and discussion

4.1. Effect of well injection parameters on IHP

Well injection parameters and its effect on the performance of the IHP is important because of its economic and environmental implications. Besides the material being injected, the two most significant injection parameters to be analysed are: injection rate and injection pressure. The decision on what type or capacity of surface pumps to use will depend on the whether the emphasis is on either higher pressure or higher rate. From the proxy model, we find that injection pressure has negligible effect on the cumulative hydrogen yield. Analysing the effect of injection rate on the cumulative hydrogen produced (CHP), a negative gradient between CHP and injection rate above 1200m^3/day as shown in Fig. 9. This implies that higher injection rates produced corresponding lower cumulative higher hydrogen. The most plausible explanation for this behaviour could be that injecting oxygen at a rate higher than 1200 m^3/day would cause the excess oxygen injected to react with the produced hydrogen to yield water.

Observing the coupled effect of injection rate and permeability changes on CHP, maximum CHP was attained at low permeability regions with the injection rate around 1200 m^3/day as observed in Fig. 10. This implies that the volume of hydrogen recovered from the IHP study strongly corelates with the quantity of oxygen injected into the reservoir. In addition, the relationship is further dependent on the reservoir permeability and porosity as will be seen in section 4.2.

4.2. Effect of reservoir parameter – porosity and permeability on IHP

An understanding of the influence of reservoir parameters on the performance of IHP is important especially as a pre-screening tool for identifying suitable reservoirs for IHP application. Using the validated proxy model developed in the previous section, a nonlinear relationship between porosity, permeability and cumulative gas produced is given in Figs. 11 and 12.

These results were obtained by keeping constant all other parameters being investigated. From the analysis, lower porosity and permeability reservoirs favours IHP process. The most plausible explanation for this observation is that lower permeability and porosity reservoirs allow for more residence time for reaction. Longer residence time favours more hydrogen producing reactions due to prolonged reaction time. Investigating the combined effect of permeability and porosity on CHP as shown in Fig. 13, it was observed that permeability had a stronger influence on the CHP than porosity. However, the computation cost of running a thermal simulation for small porosity and permeability is considerably expensive.

4.3. Effect of Well placement on performance of IHP

Assuming the location of the injection well is known, to improve the location of the Production Well in the reservoir, a data-driven technique involving the use of genetic algorithm is utilized to estimate CHP at different possible locations of {i} and {j} as shown in Fig. 14.

From the results analysed, a linear relationship was observed between the production well {i} and {j} locations and the cumulative hydrogen produced. This implies that to recover the maximum amount of CHP during the in-situ hydrogen process, the producer well should be located closer to the edge of the reservoir boundary to cover more area. Similarly for the CHP, the larger the reservoir area available to combustion, the higher the hydrogen yield from the reservoir.

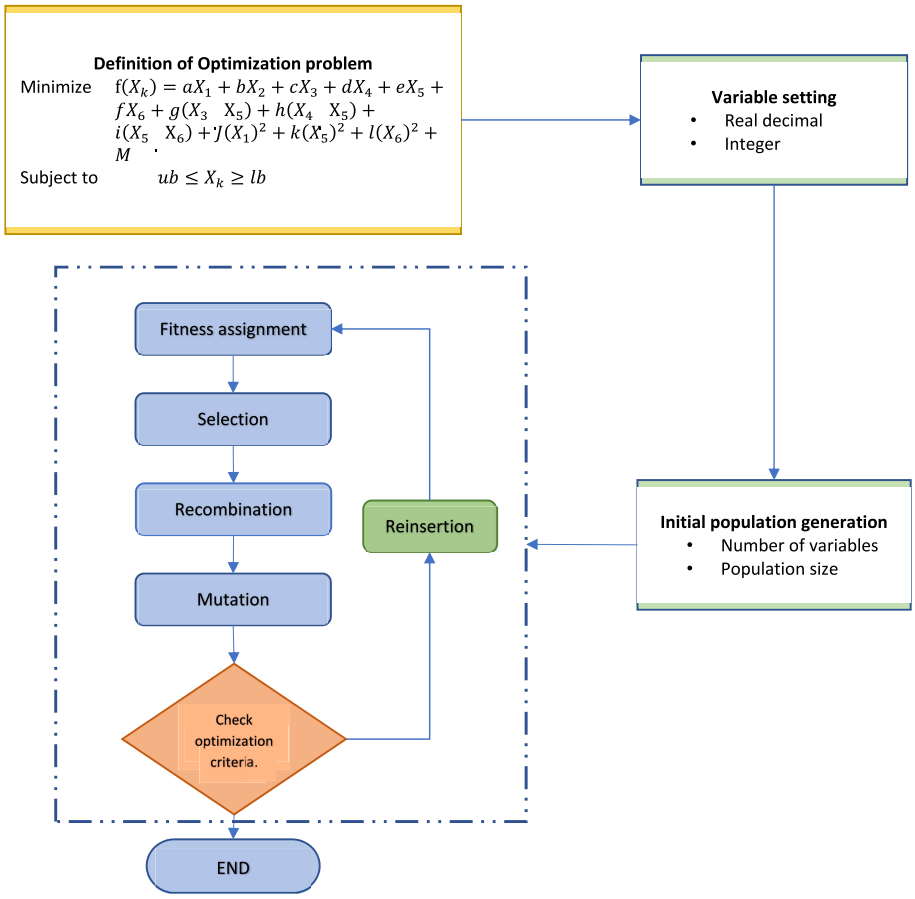

Fig. 8. Flowgorithm of genetic algorithm used in this study.

Table 6
Parameters for tuning and optimization results from the genetic algorithm.

Parameter	Value
Population size	100
Generations	100*number of variables
Reproduction	0.05*population size
Crossover function	Constraint dependent
Mutation function	Constraint dependent
Response	**Optimized parameters**
Max CHP = 1.2 E+06 m^3	$X_1 = 10$, $X_2 = 20$, $X_3 = 9$, $X_4 = 9$, $X_5 = 5000$, $X_6 = 1712.48$

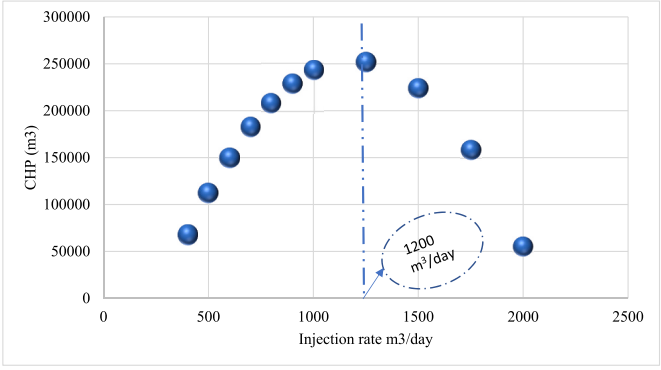

Fig. 9. Effect of Oxygen injection rate on CHP.

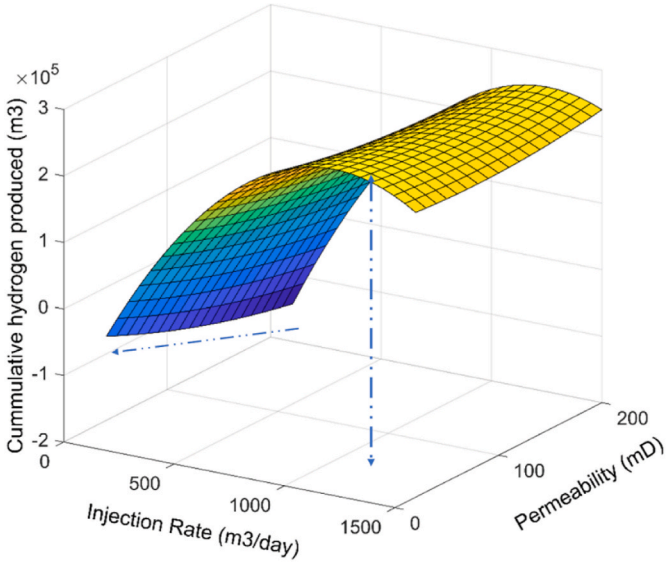

Fig. 10. Coupled effect of Injection rate and permeabilities changes on CHP.

5. Conclusion

In-situ hydrogen production (IHP) could be potentially used to extract value from depleted wells and presents an interesting solution to sustainable hydrogen need. The IHP process is dependent on several factors including reservoir rock mineralogy, combustion temperature and pressure, hydrocarbon composition and the air/oxygen injection

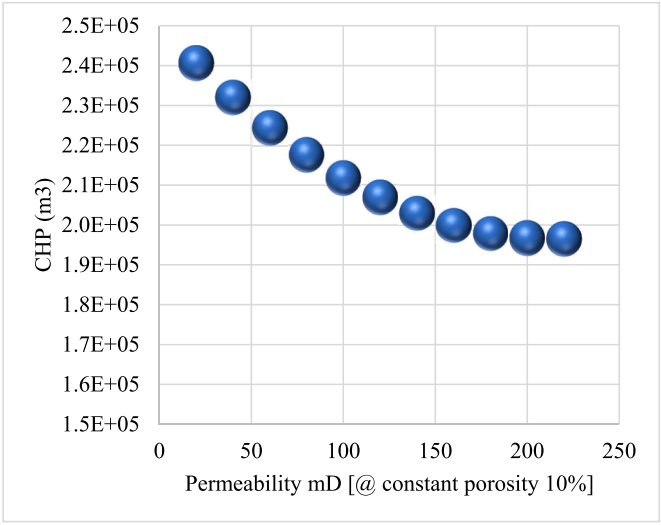

Fig. 11. Relationship between permeability and CHP.

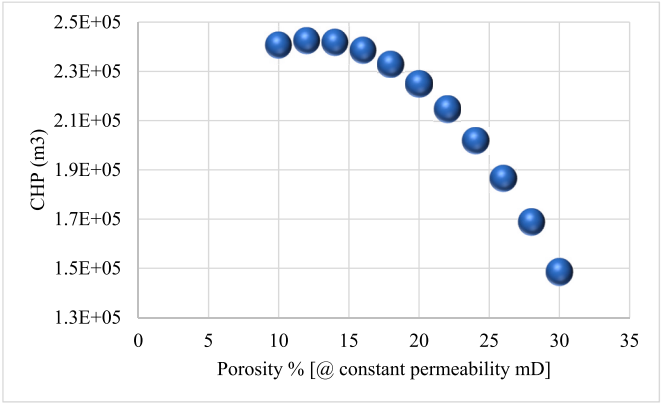

Fig. 12. Relationship between porosity and CHP.

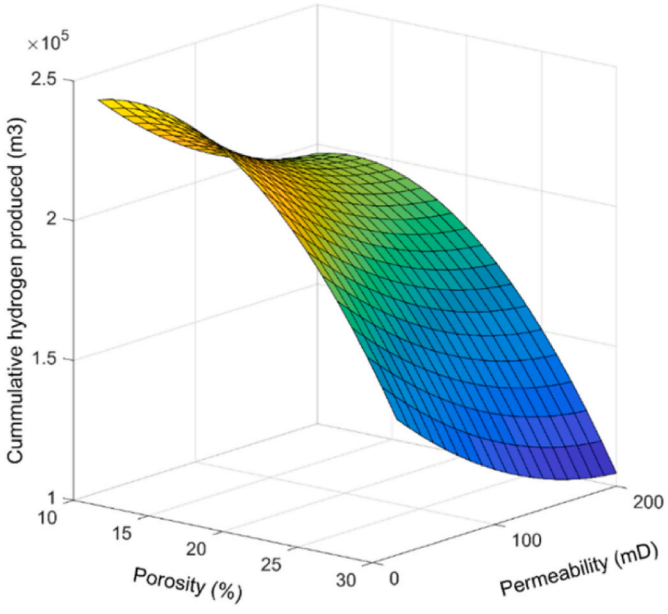

Fig. 13. Coupled effect of porosity and permeability on CHP.

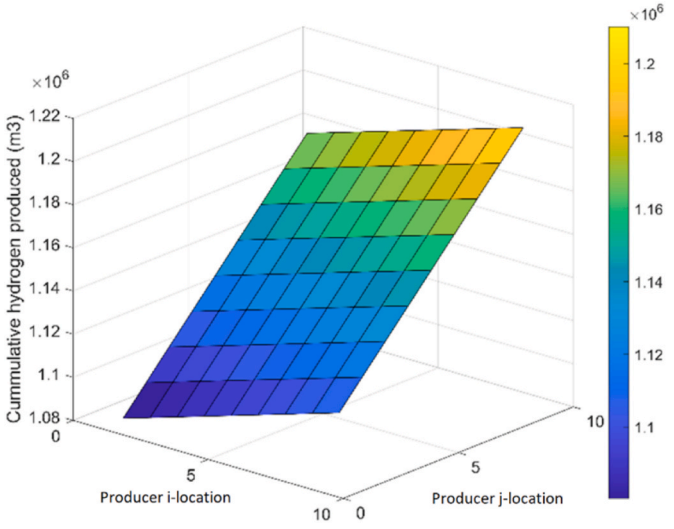

Fig. 14. Effect of Well placement on IHP performance.

ratio. This paper highlights the relative influence of reservoir properties as well as reservoir/well management decisions on hydrogen yield during in-situ hydrogen production process. Temperature and pressure play a key role during this process as in-situ hydrogen production is achieved through in-situ combustion of hydrocarbon deep in the reservoir where CO_2 is sequestered and stored in the reservoir. In addition, the influence of the reservoir and well parameters on the hydrogen yield during an in-situ hydrogen process is important as demonstrated by this study. In this study, the influence of six factors (porosity, permeability, producer I-location, producer J-location, injection rate and injection pressure) on the hydrogen yield were studied. To accomplish this, a proxy model was used as an approximate solution to full numerical simulations (CMG STARS). From the study, injection pressure was observed to have negligible effect on the cumulative hydrogen produced while oxygen injection rates above 1200 m^3/day was noted to have a negative effect on the cumulative hydrogen produced (CHP). This implies that during in-situ hydrogen process, there is an optimal injection rate beyond which excess oxygen reacts with the hydrogen produced to form water thereby reducing cumulative hydrogen yield. Another key observation from this study is that reservoirs with lower porosity and permeability favour more hydrogen yield. This is because lower permeability corelates strongly with higher reaction residence time and this allows for more hydrogen forming reactions to occur. Comparing the influence of porosity against permeability on the hydrogen yield, permeability was observed to have a stronger effect on CHP than porosity. Finally, the distance of the combustion front to producer well is also shown to affect the amount of hydrogen obtained from the in-situ hydrogen process. It is important to note that this study assumes the rate of oxygen diffusion into the reservoir is constant. Although not realistic, this assumption implies that the combustion front moves at a constant rate towards the production well. To understand the effect of production well location, this study assumes the location of the injection well is fixed. Different permutations of producer I-location and J-location were simulations using a data-driven technique to estimate CHP. It was observed that producer {i} and {j} locations furthest from the injector well had the maximum CHP which implies that hydrogen yield from the IHP process is proportional to the hydrocarbon in place. While the result of this study provides some insights on how the 6 reservoir/well parameters influence hydrogen yield, it is important to note that the numerical model was set-up using kinetic models from literature outlined in Table 3. The simulator (CMG STARS) uses finite volume approach to solve energy balance and component mass balance for each reaction which makes kinetic and heat loss data necessary. For more accurate result, the kinetic parameters need to be experimentally

obtained and validated by a well-designed laboratory investigation.

Funding

Funding for this project was received from Petroleum Technology Development Fund, under grant number PTDF/ED/PHD/PPI/1028/17. The funders had no role in study design, data collection and analysis, decision to publish, or preparation of the manuscript.

CRediT authorship contribution statement

Princewill Ikpeka: Writing – review & editing, Writing – original draft, Visualization, Methodology, Investigation, Funding acquisition, Formal analysis, Data curation, Conceptualization. **Emmanuel Alozieuwa:** Validation, Formal analysis, Data curation. **Ugochukwu I. Duru:** Resources, Formal analysis, Data curation. **Johnson Ugwu:** Supervision, Resources, Project administration.

Declaration of competing interest

The authors declare the following financial interests/personal relationships which may be considered as potential competing interests.

Princewill Ikpeka reports financial support was provided by Petroleum Technology Development Fund. If there are other authors, they declare that they have no known competing financial interests or personal relationships that could have appeared to influence the work reported in this paper.

Appendix A. Supplementary data

Supplementary data to this article can be found online at https://doi.org/10.1016/j.ijhydene.2024.07.180.

References

[1] Ball M, Weeda M. The hydrogen economy - vision or reality? Int J Hydrogen Energy 2015;40:7903–19. https://doi.org/10.1016/j.ijhydene.2015.04.032.
[2] da Silva Veras T, Mozer TS, da Costa Rubim Messeder dos Santos D, da Silva César A. Hydrogen: trends, production and characterization of the main process worldwide. Int J Hydrogen Energy 2017;42:2018–33. https://doi.org/10.1016/j.ijhydene.2016.08.219.
[3] Ali Khan MH, Daiyan R, Neal P, et al. A framework for assessing economics of blue hydrogen production from steam methane reforming using carbon capture storage & utilisation. Int J Hydrogen Energy 2021;46:22685–706. https://doi.org/10.1016/j.ijhydene.2021.04.104.
[4] Gillick SR, Babaei M. In-situ hydrogen production from natural gas wells with subsurface carbon retention. SPE J 2024;29:2119–29. https://doi.org/10.2118/219449-PA.
[5] Kapadia PR, Kallos MS, Gates ID. Potential for hydrogen generation from in situ combustion of Athabasca bitumen. Fuel 2011;90:2254–65. https://doi.org/10.1016/j.fuel.2011.02.038.
[6] Yang S, Huang S, Jiang Q, et al. Experimental study of hydrogen generation from in-situ heavy oil gasification. Fuel 2022;313:122640. https://doi.org/10.1016/j.fuel.2021.122640.
[7] Song P, Li Y, Yin Z, Yuan Q. Hydrogen generation from heavy oils via in-situ combustion gasification. SPE West. Reg. Meet 2023:D031S007R003.
[8] Song P, Li Y, Yin Z, et al. Simulation of hydrogen generation via in-situ combustion gasification of heavy oil. Int J Hydrogen Energy 2024;49:925–36. https://doi.org/10.1016/j.ijhydene.2023.09.248.
[9] Okere CJ, Sheng JJ. A new modelling approach for in-situ hydrogen production from heavy oil reservoirs: sensitivity analysis and process mechanisms. Energy 2024;302:131817. https://doi.org/10.1016/j.energy.2024.131817.
[10] Yan Y, Gonzalez-Cortes S, AlMegren H, et al. Hydrogen production from crude oil with fine iron particles through microwave-initiated catalytic dehydrogenation promoted by emulsified feed. Int J Hydrogen Energy 2018;43:23201–8. https://doi.org/10.1016/j.ijhydene.2018.10.141.
[11] Yuan Q, Jie X, Ren B. Hydrogen generation in crushed rocks saturated by crude oil and water using microwave heating. Int J Hydrogen Energy 2022;47:20793–802. https://doi.org/10.1016/j.ijhydene.2022.04.217.
[12] Hajdo LE, Hallam RJ, Vorndran LDL. Hydrogen generation during in-situ combustion. In: SPE California regional meeting. Society of Petroleum Engineers; 1985.
[13] Hallam RJ, Hajdo LE, Donnelly JK, Baron PR. Thermal recovery of bitumen at Wolf Lake. SPE Reservoir Eng 1989;4:178–86.
[14] Ikpeka P, Ugwu J, Russell P, Pillai G. Insitu hydrogen production from hydrocarbon reservoirs-what are the key challenges and prospects?. In: 1st geoscience & engineering in energy transition conference; 2020. p. 1–5.
[15] Yu M, Wang K, Vredenburg H. Insights into low-carbon hydrogen production methods: green, blue and aqua hydrogen. Int J Hydrogen Energy 2021;46:21261–73. https://doi.org/10.1016/j.ijhydene.2021.04.016.
[16] Salahshoor S, Afzal S. Subsurface technologies for hydrogen production from fossil fuel resources: a review and techno-economic analysis. Int J Hydrogen Energy 2022. https://doi.org/10.1016/j.ijhydene.2022.08.202.
[17] Ifticene MA, Yan K, Yuan Q. Fueling a carbon-zero future: igniting hydrogen production from petroleum reservoirs via in-situ combustion gasification. Energy Convers Manag 2023;298:117770. https://doi.org/10.1016/j.enconman.2023.117770.
[18] Liu Z, Pu W, Zhao X, et al. Combustion tube experiments on key factors controlling the combustion process of air injection with light oil reservoir. Geoenergy Sci Eng 2023;224:211611. https://doi.org/10.1016/j.geoen.2023.211611.
[19] Ikpeka PM, Ugwu JO. In situ hydrogen production from hydrocarbon reservoirs - modelling study. RSC Adv 2023;13:12100–13. https://doi.org/10.1039/d3ra01762a.
[20] Okere CJ, Sheng JJ, Ikpeka PM. Maximizing hydrogen yield: pioneering gas injection for enhanced light oil reservoir utilization. 2024, D021S011R006.
[21] Zhang J, Li X, Chen H, et al. Hydrogen production by catalytic methane decomposition: carbon materials as catalysts or catalyst supports. Int J Hydrogen Energy 2017;42:19755–75. https://doi.org/10.1016/j.ijhydene.2017.06.197.
[22] Storey BM, Worden RH, McNamara DD. The geoscience of in-situ combustion and high-pressure air injection. Geosci 2022;12. https://doi.org/10.3390/geosciences12090340.
[23] Ranjbar M. Improvement of medium and light oil recovery with thermocatalytic in situ combustion. J Can Pet Technol 1995;34:25–30. https://doi.org/10.2118/95-08-02.
[24] Ismail NB, Hascakir B. Impact of asphaltenes and clay interaction on in-situ combustion performance. Fuel 2020;268:117358. https://doi.org/10.1016/j.fuel.2020.117358.
[25] Akkutlu IY, Yortsos YC. The dynamics of in-situ combustion fronts in porous media. Combust Flame 2003;134:229–47. https://doi.org/10.1016/S0010-2180(03)00095-6.
[26] Smith EK, Barakat SM, Akande O, et al. Subsurface combustion and gasification for hydrogen production: reaction mechanism, techno-economic and lifecycle assessment. Chem Eng J 2024;480:148095. https://doi.org/10.1016/j.cej.2023.148095.
[27] Askarova A, Afanasev P, Popov E, et al. SPE-219092-MS in situ generation of clean hydrogen in gas reservoirs: experimental and numerical study. 2024.
[28] Greaves M, Young TJ, El-Usta S, et al. Air injection into light and medium heavy oil reservoirs: combustion tube studies on west of shetlands clair oil and light Australian oil. Chem Eng Res Des 2000;78:721–30. https://doi.org/10.1205/026387600527905.
[29] Niz-Velásquez E, Moore RG, Van Fraassen KC, et al. Experimental and numerical modeling of three-phase flow under high-pressure air injection. SPE Reservoir Eval Eng 2010;13:782–90. https://doi.org/10.2118/127719-PA.
[30] Alamatsaz A, Moore GR, Mehta SA, Ursenbach MG. Analysis of dry, wet and superwet in situ combustion using a novel conical cell experiment. Fuel 2018;234:482–91. https://doi.org/10.1016/j.fuel.2018.06.108.
[31] Alexander JD, Martin WL, Dew JN. Factors affecting fuel availability and composition during in situ combustion. J Petrol Technol 1962;14:1154–64. https://doi.org/10.2118/296-pa.
[32] Okere CJ, Sheng JJ. Review on clean hydrogen generation from petroleum reservoirs: fundamentals, mechanisms, and field applications. Int J Hydrogen Energy 2023;48:38188–222. https://doi.org/10.1016/j.ijhydene.2023.06.135.
[33] Kok MV, Keskin C. Comparative combustion kinetics for in situ combustion process. Thermochim Acta 2001;369:143–7. https://doi.org/10.1016/S0040-6031(00)00765-6.
[34] Kenyon D. Third SPE comparative solution project: gas cycling of retrograde condensate reservoirs. J Petrol Technol 1987;39:981–97. https://doi.org/10.2118/12278-PA.
[35] Ikpeka P, Ugwu J, Russell P, Pillai G. Performance evaluation of machine learning algorithms in predicting dew point pressure of gas condensate reservoirs. SN Appl Sci 2020;2:1–14. https://doi.org/10.1007/s42452-020-03811-x.
[36] Trento LM, Tsourlos P, Gerhard JI. Time-lapse electrical resistivity tomography mapping of DNAPL remediation at a STAR field site. J Appl Geophys 2021;184:104244. https://doi.org/10.1016/j.jappgeo.2020.104244.
[37] Ferreira SLC, Bruns RE, Ferreira HS, et al. Box-Behnken design: an alternative for the optimization of analytical methods. Anal Chim Acta 2007;597:179–86. https://doi.org/10.1016/j.aca.2007.07.011.
[38] Adegbesan KO, Donnelly JK, Moore RG, Bennion DW. Low-temperature-oxidation kinetic parameters for in-situ combustion: numerical simulation. SPE Reserv Eng (Society Pet Eng 1987;2:573–82. https://doi.org/10.2118/12004-PA.

[39] Yang X, Gates ID. Combustion kinetics of Athabasca bitumen from 1D combustion tube experiments. Nat Resour Res 2009;18:193–211. https://doi.org/10.1007/s11053-009-9095-z.
[40] Guntermann K, Breidung P, Fuhrmann F, et al. Pressure-swinging underground gasification. Theoretical and experimental investigations of gasification. Phase 3. Druckwechsel-Unter-Tage-Vergasung. Theoretische und experimentelle Untersuchungen zum Vergasungsvorgang untertage. Phase 1984;3:250.
[41] Babushok VI, Dakdancha AN. Global kinetic parameters for high-temperature gas-phase reactions. Combust Explos Shock Waves 1993;29:464–89. https://doi.org/10.1007/BF00782974.
[42] Johnson JrLA, Fahy LJ, Romanowski LJ, et al. An echoing in-situ combustion oil recovery project in a Utah tar sand. J Petrol Technol 1980;32:295–305. https://doi.org/10.2118/7511-PA.
[43] Liu Hui, Chen Zhangxin, Guo Xiaohu, Lihua Shen. Development of a Scalable Thermal Reservoir Simulator on Distributed-Memory Parallel Computers. Fluids 2021;6(11):395. https://doi.org/10.3390/fluids6110395.